HHS Public Access

Anatomical and fMRI-network comparison of multiple DLPFC targeting strategies for repetitive transcranial magnetic stimulation treatment of depression

V.A. Cardenas[a], **J.V. Bhat**[a,b], **A.M. Horwege**[a], **T.J. Ehrlich**[a,c], **J. Lavacot**[a], **D.H. Mathalon**[d,e], **G.H. Glover**[f], **B.J. Roach**[d,g], **B.W. Badran**[h], **S.D. Forman**[i,j], **M.S. George**[h,k], **M.E. Thase**[l,m], **J.A. Yesavage**[a,n], **D. Yurgelun-Todd**[o,p], **A.C. Rosen**[a,n,*]

[a]Veterans Affairs Palo Alto Health Care System, Palo Alto, CA, USA

[b]Palo Alto Veterans Institute for Research, Palo Alto, CA, 94304, USA

[c]University of Michigan, Ann Arbor, MI, USA

[d]Mental Health Service, San Francisco Veterans Affairs Health Care System, University of California, San Francisco, San Francisco, CA, USA

[e]Department of Psychiatry, University of California, San Francisco, San Francisco, CA, USA

[f]Department of Radiology, Stanford University, Stanford, CA, USA

[g]Northern California Institute for Research and Education, San Francisco Veterans Affairs Medical Center, University of California, San Francisco, San Francisco, CA, USA

[h]Brain Stimulation Division, Department of Psychiatry, Medical University of South Carolina, Charleston, SC, USA

[i]Department of Veterans Affairs, Veterans Affairs Medical Center, Pittsburgh, PA, USA

[j]Western Psychiatric Institute and Clinic, University of Pittsburgh School of Medicine, Pittsburgh, PA, USA

[k]Ralph H. Johnson VA Medical Center, Charleston, SC, USA

[l]VISN4 Mental Illness Research, Education, and Clinical Center at the Corporal Michael J. Crescenz VA Medical Center, Philadelphia, PA, 19104, USA

*Corresponding author. Palo Alto VAHCS, 3801 Miranda Ave (151Y), Palo Alto, CA, 94304-1207, USA. rosena@stanford.edu (A.C. Rosen).

mDepartment of Psychiatry, Perelman School of Medicine, University of Pennsylvania, Philadelphia, PA, USA

nDepartment of Psychiatry and Behavioral Sciences, Stanford University School of Medicine, Stanford, CA, USA

oRocky Mountain Network Mental Illness Research Education and Clinical Centers (VISN 19), VA Salt Lake City Health Care System, Salt Lake City, UT, USA

pDepartment of Psychiatry, University of Utah School of Medicine, Salt Lake City, UT, USA

Abstract

Background: The efficacy of repetitive transcranial magnetic stimulation (rTMS) for depression may vary depending on the subregion stimulated within the dorsolateral prefrontal cortex (DLPFC). Clinical TMS typically uses scalp-based landmarks for DLPFC targeting, rather than individualized MRI guidance.

Objective: In rTMS patients, determine the brain systems targeted by multiple DLPFC stimulation rules by computing several surrogate measures: underlying brain targets labeled with connectivity-based atlases, subgenual cingulate anticorrelation strength, and functionally connected networks.

Methods: Forty-nine patients in a randomized controlled trial of rTMS therapy for treatment resistant major depression underwent structural and functional MRI. DLPFC rules were applied virtually using MR-image guidance. Underlying cortical regions were labeled, and connectivity with the subgenual cingulate and whole-brain computed.

Results: Scalp-targeting rules applied post hoc to these MRIs that adjusted for head size, including Beam F3, were comparably precise, successful in directly targeting classical DLPFC and frontal networks, and anticorrelated with the subgenual cingulate. In contrast, all rules involving fixed distances introduced variability in regions and networks targeted. The 5 cm rule targeted a transitional DLPFC region with a different connectivity profile from the adjusted rules. Seed-based connectivity analyses identified multiple regions, such as posterior cingulate and inferior parietal lobe, that warrant further study in order to understand their potential contribution to clinical response.

Conclusion: EEG-based rules consistently targeted DLPFC brain regions with resting-state fMRI features known to be associated with depression response. These results provide a bridge from lab to clinic by enabling clinicians to relate scalp-targeting rules to functionally connected brain systems.

Keywords

1. Introduction

An increasing number of patients with treatment resistant major depression (TRMD) are receiving repetitive transcranial magnetic stimulation therapy (rTMS) [1–3]. The most

common method of rTMS therapy places a treatment coil on the patient's scalp over the frontal lobe to induce focal electromagnetic fields that modulate the underlying dorsolateral prefrontal cortex (DLPFC) and functionally connected networks [4]. Recent meta-analyses and large-scale studies estimate that only about a third of TRMD patients treated with rTMS therapy achieve acute remission, typically defined as scoring <10 on the 24-item Hamilton Scale for Depression (HSRD) [5,6], with another third achieving acute response (>50% reduction in symptoms). Because the targeted frontal lobe comprises multiple distinct anatomical sub-regions [7] and variability in depression response may relate to stimulus coil placement [8–11], several groups have proposed optimal anatomical or functional DLPFC targets. While these "optimal" targets were derived from different cohorts, they are strikingly similar and clustered closely together within DLPFC [12]. What then are the differences between these targets, and how can a clinician best approximate these targets in the absence of MRI-neuronavigation?

Abnormal DLPFC function has been implicated in depression [13–16], and thus its use as an rTMS target has a long history [17,18]. The DLPFC is functionally defined as the cortical area involved in cognitive control and is classically attributed to anatomical Brodmann areas 9 and 46 (BA 9/46) [19]. In the vast majority of clinical cases and the early published, sham-controlled, clinical rTMS trials, the DLPFC was identified relative to motor cortex. Specifically, clinicians identified the scalp location where TMS evoked a thumb contraction (the motor hotspot), then treated at a fixed distance anterior to this location. While early rTMS studies typically moved 5 cm anteriorly (the "5-cm rule" [17,18]), later work demonstrated that the DLPFC was missed in up to a third of patients [11,20–22], prompting variations of the rule that moved farther anterior [9,23]. Later MRI-guided neuronavigation work suggested that moving about 7 cm anterior to the motor hotspot would target DLPFC more accurately [24,25].

Critics point out that fixed distance targeting rules do not account for individual head morphometry, and targeting rules that adjust for head size target DLPFC more accurately [26]. When neuronavigation is available, each subject's MRI is coregistered to a standard brain template, typically from the Montreal Neurological Institute (MNI) [27,28], thus adjusting for head size and shape. The stimulation site can then be projected to the scalp from an MNI coordinate chosen from a published study, e.g. Refs. [10,11,29], or derived from an individualized imaging analysis [9,30–32]. However, neuronavigation is rarely used in rTMS clinics because the additional implementation burden is not justified by the inconsistent improvement in depression outcomes compared to fixed-rule targeting [29,33]. In the absence of MRI-guided neuronavigation, targeting at the EEG F3 electrode location [34] or the Beam F3 simplified scalp tracing scheme [35] are recommended [36], as these techniques make simple adjustments for head size [37].

Based on the idea that depression response is due to both direct DLPFC and downstream modulation of connected brain regions, targeting based on the synchronous activation of distinct brain regions is increasingly popular [38,39]. Multiple studies show that stimulation at sites with maximal fMRI anticorrelation with the subgenual cingulate [8–10] is related to HSRD improved response [31,40,41]. Expanding this idea, an examination of whole brain connectivity with the stimulation sites of depression responders might reveal which

networks are modulated during treatment for depression [42,43], and identify regions that are not directly stimulated but could moderate clinical response. Connectivity-based atlases [7,44] may also identify stimulated networks.

This study uses MR image guidance software to virtually define stimulation locations using several fixed-distance rules and rules that adjust for head size for a cohort of patients with treatment resistant major depression (TRMD) who participated in a clinical trial (CSP556) that treated using the 6-cm fixed distance rule [23]. Several surrogate markers of the brain systems that would be modulated in a clinic were assessed: the precision in targeting DLPFC, the degree of anticorrelation with the subgenual cingulate, and connected functional networks. We hypothesized that rules adjusted for head size would reach more consistent anatomy and networks, the 6 and 7 cm rules would target BA 9 and 46 most consistently of the fixed distance rules, and that MNI-coordinate-defined targets would be most consistent. Our work identifies which scalp-based targeting rules best approximate optimized MNI-coordinate-defined targets, and establishes the correspondence between atlases of networks derived from healthy samples [7,44], and networks in our depressed cohort. Our current results provide a bridge for translation from lab to clinic by showing how different rules target underlying anatomy and different brain systems, potentially enabling clinicians to choose a targeting strategy to best treat individual patient symptoms.

2. Material and methods

Of the 342 patients assessed for eligibility in the original study, 164 were randomized to the larger sham-controlled clinical trial of rTMS (ClinicalTrials.gov ID: NCT01191333). Forty-nine Veterans with TRMD from the six centers with 3T MRIs were recruited for this imaging sub-study, see Table 1 for basic demographic information. This study was approved by the Veterans Administration Central Institutional Review Board and the Research and Development Committee of the Veterans Affairs Palo Alto Health Care System. Participants signed an informed consent document and were paid for their participation in the study; see previous publications for full inclusion and exclusion criteria [23,45]. Structural MRI and resting state fMRI were collected (see Supplement for acquisition details).

2.1. MRI analysis

2.1.1. Identifying the virtual scalp and brain targets—Each subject's T1-image was loaded into Brainsight image-guidance software (Rogue Research, Montreal Canada). Registration to MNI-space occurred after manual identification of the anterior and posterior commissures, interhemispheric plane, and bounding box of the brain. All registrations were verified manually. A three-dimensional reconstruction of each participant's scalp and brain was derived from their MRI and used to define the virtual scalp and brain targets, shown in Supplemental Fig. S1.

2.1.2. Fixed distance targeting rules—The idealized motor hotspot was identified by projecting a perpendicular line up to the scalp from the omega-shaped hand knob in the motor cortex [46,47]. From the idealized motor hotspot, the treatment location was determined by tracing a fixed distance forward, parallel to the interhemispheric fissure and accounting for curvature, beginning with 5 cm and increasing by 1 cm increments until

targets were outside Brodmann's areas 9 or 46 as defined by a popular atlas [48], resulting in 5, 6, 7, 8, 9, and 10 cm rules. A line was projected down from a virtual treatment coil to determine the cortical location corresponding to each target.

2.1.3.   Adjusted targeting rules—The following brain targets were identified for each subject: the ideal location for the EEG-F3 electrode (MNI: −51, 51, 44; see Supplement for details); the target reported by Fitzgerald 2009 [24] as optimal (MNI: −45, 45, 35); the Fox 2012 [10] DLPFC target (MNI: −38, 44, 26); the border between BA 9 and BA 46 (BA9/46), and Beam-F3 traced virtually [35]. When targets defined by MNI coordinates were located outside the cortical ribbon due to head shape variation, the target was nudged perpendicular to the scalp until it intersected the cortex. For the BA9/46 target, an atlas of Brodmann areas [48] was overlaid on the subject's MRI and the center of the BA 9/46 border manually approximated. For Beam-F3, the tragus-tragus distance, nasion-inion distance, and head circumference were measured on the subject's 3D reconstruction using Brainsight's 3D ruler and input at http://clinicalresearcher.org/F3/ to calculate the Beam F3 scalp tracing distances (using the adjusted y value), which were then virtually traced to locate the scalp target. The Beam F3 scalp target was nudged perpendicular to the scalp until the target intersected the cortex.

2.1.4.   Identifying the brain target for applied 6 cm rule—Stimulation was delivered 6 cm anterior to the motor hotspot (see Supplement); each patient had a cloth cap marked with the treatment location (MagVenture, Farum, Denmark) for re-use by treaters to consistently position the treatment coil. For each patient, the treatment location identified by the fiducial marker was projected to the underlying brain surface using Brainsight.

2.1.5.   Dispersion and labeling of targets—For each rule, the MNI coordinates of the cortical targets for the 49 subjects are used to calculate the sample variance-covariance matrix. The eigenvectors of this matrix define the major and minor axes of an error ellipsoid [49]. The error ellipsoid for each rule was calculated using unscaled eigenvalues, which corresponds to an ellipse centered at the average target location, with axes lengths representing one standard deviation. We used Box's M Test to check for the homogeneity of covariance between different targeting rules.

Each target's MNI coordinate was compared to the HCP atlas [7], and when the coordinate was unlabeled a search was made in the surrounding 1 cm radius neighborhood to find the closest matching label, as defined by Euclidean distance. A similar process was used to find the closest matching Yeo-7 Network [44] underlying each target's MNI coordinate. To test whether there was a relationship between targeting rule and HCP or Yeo-7 label, χ^2 tests for independence were conducted on the subset of labels for which the test was valid (excluding labels with count<5).

2.1.6.   Resting-state fMRI analyses—Preprocessing of resting state fMRI (see Supplement) used a standard pipeline [50–53] as detailed in the Supplement; one patient's fMRI failed quality checks and was excluded from fMRI analyses. A single 10 mm sphere centered at the subgenual region (6, 16, −10) as previously reported [10] was masked to exclude voxels falling outside of the brain. The functional connectivity between this

subgenual region and a 10 mm sphere centered at each cortical target for each of the remaining 48 patients and each rule was derived. Specifically, the residual BOLD time courses from voxels within the subgenual seed region were averaged and correlated with the average BOLD timecourse of each cortical target. The average BOLD timecourse of each cortical target was also correlated with every other brain voxel to produce first-level correlation maps. Correlation coefficients were transformed using the Fisher z-transformation.

For each rule, the average r-to-z correlation at each voxel was compared to 0 and T-statistics computed (AFNI's 3dttest++-Clustsim option) to identify functional clusters [54,55] significant at $\alpha = 0.05$ (bi-sided threshold at $P < 0.001$ [56], faces or edges touch [57–59]). Cluster peaks were labeled using the HCP structural atlas [7] and Yeo network atlas [44]. Dice coefficients [60] between the Yeo-7 networks and the network defined by the significant clusters were computed to identify the overlap (range: 0–1) between the resting-state networks functionally connected to each target estimated from TRMD patients and established resting-state networks estimated from healthy controls. The Supplement describes an alternate method for identifying the correspondence between networks evoked by each rule and established networks.

3. Results

3.1. Dispersion and labeling of targets

Green error ellipses representing the location and spatial dispersion of targets located using fixed-distance rules (i.e., fixed rules), rules adjusting for head size (i.e., adjusted rules), and the 6 cm rule applied in the parent trial (i.e., applied 6 cm rule) are shown in Fig. 1a. The 8 cm fixed rule is located closest to the adjusted rules, suggesting that the 5 and 6 cm rules popularly used in clinical treatment target a different region of the brain from the optimized rules. As hypothesized, the fixed distance rules have about twice the error ellipse volume (mean ± SD: 654 ± 17 mm^3) than the adjusted rules (301 ± 75 mm^3), with the increase likely due to head size variability. The variability of target placement of the 6 cm rule implemented in CSP556 was far greater, with an error ellipse volume of 919 mm^3, and the location also appeared shifted laterally. This may occur because the structurally defined hand knob used in our rules may be less variable in location than the functionally defined hotspot [61,62]. To test this, we compared the MNI-coordinates of the hand knob location and the motor hotspot fiducial from CSP556. As suspected, the hand knob and motor hotspot coordinates were significantly different (MANOVA, $P < 0.001$) and the error ellipse volume for the hand knob was much smaller (611 mm^3) compared to the motor hotspot (1012 mm^3, Fig. S2, Supplement). The average distance between the applied 6 cm rule and the motor hotspot was 5.8 cm and between the virtual 6 cm rule and the hand knob was 6.2 cm, lending additional validity to both the applied and virtual rules, with the caveat that they were measured from different starting positions. Box's M test showed that covariance matrices were equivalent for all fixed rules, for all adjusted rules, and that the covariances for the fixed, adjusted, and applied 6 cm rule were not equivalent to each other (Fig. 2).

Although there was substantial variability in the regions targeted with fixed distance rules, all fixed distance rules targeted classical DLPFC (9/46) some of the time, as shown in Fig.

3 (see Supplemental Tables S1 and S2 for a detailed breakdown). The 5 cm rule was least accurate, with the bulk of 5 cm targets in Areas 8 and 6–8 (described as a transitional DLPFC region in Ref. [7]). Progressively anterior fixed distance rules targeted Areas 8 and 6–8 less frequently and shifted to Areas 9 and 46, the classical DLPFC. Only a small fraction of 5 and 6 cm rule targets were in premotor/Area 6. All the rules except the 9 cm rule targeted a small number of patients in more inferior frontal regions (Areas 44, 47, IFS).

As expected, rules adjusted for head size more consistently targeted regions classically considered to be DLPFC (Areas 9,46) with few errors, as shown in Fig. 3. The BA9/46 rule targeted a small percentage in the transitional DLPFC (Areas 8 and 6–8). All other adjusted rules targeted ventrally in inferior frontal cortex in a small fraction of cases.

The fixed distance rules also introduced large variability in the networks targeted, as shown in Fig. 3. Specifically, the bulk of 5 cm targets were in the DMN (76%) with a lesser number (20%) in frontoparietal and a small fraction in ventral (2%) and dorsal (2%) attention networks. Moving anteriorly from the 5 cm rule to the 8 cm rule, the percentage of targets located in the DMN decreased while the percentage located in the ventral attention network (comprised of the salience and cingulo-opercular task control networks, [63,64]) increased. The percentage of targets located within the frontoparietal network increased in the 9 cm (51%) and 10 cm rules (71%), and fewer targets were located in the ventral attention network. The 6 cm applied rule deviated from that pattern with more targets located within the frontoparietal network (64%) than any fixed rule except the 10 cm rule.

As seen in Fig. 3, most adjusted rule targets were located within the ventral attention network (range: 51–80%), with a small number located within the DMN (2–4%) and the remaining within the frontoparietal network (range: 14–47%).

The χ^2 tests for rule by cortical area showed that the percentage of targets in classical DLPFC and transitional DLPFC differed for every rule, i.e. the 5 cm rule preferentially targeted transitional DLPFC while all other rules preferentially targeted classical DLPFC. For the test of rule by network, superscript letters on Fig. 3a denote which networks were differently targeted for each rule. The 5 cm rule preferentially targets the default mode network, because the % of targets in the ventral attention, frontoparietal, and default mode networks are all significantly different. In contrast, the adjusted rules all preferentially target the ventral attention compared to the default mode network. The χ^2 test results for label by rule in Fig. 3b show that nonadjacent fixed distance rules tended to target different anatomy and networks. Of note, the 7 and 8 cm rules showed no differences in direct targeting from any of the adjusted rules and the adjusted rules all targeted the same anatomy and networks, as outlined in Fig. 3.

3.2. Resting state fMRI analyses

Fig. 4 illustrates that the virtual rules differed with respect to their magnitude of anticorrelation with the subgenual cingulate, as confirmed by a repeated measures general linear model (P = 0.01). Post-hoc analysis of all pairwise t-tests, corrected for multiple comparisons, revealed that average r-to-z for the applied 6 cm, 7 cm, and all adjusted rules was not significantly different from any rule. The 5, 6, 8, 9, and 10 cm rules were

less anticorrelated compared to one or more of the adjusted rules (Fig. 4). Somewhat surprisingly, the average anticorrelation tended to increase as rules moved farther anterior (range: 0.04 to −0.09). Despite the relative uniformity of anatomical structures and Yeo networks targeted by the adjusted rules, there was striking variability in the degree of anticorrelation with the subgenual cingulate. The strongest average anticorrelations were observed in the Fox 2012 (−0.16) and Fitzgerald 2009 (−0.15) rules.

Fig. 1 shows the average resting-state networks connected to the virtually traced targets for each rule and the overlap with selected Yeo-7 networks. Cluster peak results are summarized here; the Supplement contains details of the peak analyses (Tables S3 and S4, and detailed discussion), overlaps of the remaining networks (Fig. S3), and an alternate analysis of network overlap (Fig. S4).

Although at first glance the pattern of resting-state connectivity looks similar across the fixed rules, several differences are worth noting. The most striking pattern emerges when examining the overlap of positive connectivity clusters with the Yeo-7 networks across the fixed rules (red bars in Fig. 1c). For the 5 cm rule, the overlap with the ventral attention network is nearly zero and the overlap with the DMN of around 0.4. As the targets move anteriorly, the ventral attention overlap increases while the DMN overlap decreases, with the maximum ventral attention and minimum DMN overlap observed for the 8 cm rule. The pattern reverses for the 9 and 10 cm rules. All fixed rule targets show positive connectivity that overlaps with the frontoparietal network to a relatively consistent degree (overlap range: 0.26–0.38). Negative overlap (blue bars in Fig. 1c) with the somatomotor network is greatest for the 5 cm rule and decreases anteriorly, although cluster peaks within the somatomotor network appear for all fixed rules.

The positive connectivity of all adjusted rules overlaps with the frontoparietal (overlap range: 0.33–0.67) and the ventral attention (range: 0.37–0.79) networks. While all adjusted rules overlapped with the dorsal attention network to some degree (overlap range: 0.06– 0.20), no cluster peaks were localized there. With respect to negative connectivity, all adjusted rules except BA9/46 resulted in large clusters in ventromedial prefrontal limbic regions encompassing the subgenual cingulate. The bulk of the negative cluster peaks were in lateral temporal, posterior cingulate, and inferior parietal nodes of the DMN, with overlap between negative connectivity clusters and the DMN ranging from 0.14 to 0.19. None of the fixed rules show notable negative connectivity with the DMN.

4. Discussion

This study demonstrated four systematic relationships between scalp targets, connectivity-based brain atlases, and functional connectivity in TMS patients with TRMD which have implications for clinical rTMS implementation. First, all scalp targeting rules that adjusted for head size were comparable to one another on all derived measures. Failure to adjust for head size introduces variability and the applied 6 cm rule introduced far greater variability. Second, all the adjusted rules tested here were successful in directly targeting classical DLPFC and frontal networks; they were also functionally correlated to varying degrees with brain regions overlapping the frontoparietal and ventral attention networks

and anticorrelated with brain regions overlapping the DMN. Third, the 5 cm rule directly targeted a region quite different from all other rules, specifically a transitional DLPFC region (area 8 and 6–8); its targets were functionally correlated with regions overlapping the default mode and frontoparietal networks and anticorrelated with regions within the ventral attention and somatomotor networks, and showed smaller anticorrelation with the subgenual cingulate than the adjusted rules. Finally, the seed-based connectivity analyses identified multiple regions, such as posterior cingulate and inferior parietal lobe, that were functionally connected to the virtual targets and warrant further study in order to understand their potential contribution to clinical response.

Targets localized using head size adjusted rules were more spatially focused across patients, while the implemented 6 cm rule had a greater than expected spatial dispersion and a different location from the virtually traced 6 cm rule. The error ellipse volume for the fixed distance targets is more than double that of the adjusted targets, and we would expect even larger spatial dispersion if our sample had included more women and variability in age [65]. There are likely multiple contributors to the disagreement between virtual and applied 6 cm rule targets, including errors in motor hotspot localization and the use of a marking plate (Magventure model #9016B050) designed to make the 6 cm tracing more consistent, but instead introduced a lateral shift due to the TMS coil weight. Finally, we concur with reports that maintaining any target without MR image-guidance feedback can be problematic [66].

Our results are consistent with reports that the 5 cm rule misses BA 9 or 46 in 30–70% of patients [22,62] and instead targets BA 6 or 8. BA 6 and 8 are traditionally considered premotor cortex, but atlases derived from connectivity-analyses of HCP images [7,44] instead classify area 8 and a new area 6–8 as a transitional DLPFC region. Using these atlases, the 5 cm rule targeted about 85% of patients in the transitional DLPFC and DMN, in contrast to about 40% for the 6 cm rule, while the adjusted rules targeted Areas 9 and 46 of the classically defined DLPFC in 96–98% of patients. The transitional DLPFC is close to a region with a symptomatically different pattern of rTMS clinical depression response described as anxiosomatic [67]. Taken together with the report that only patients stimulated in BA 6 consistently fail to achieve remission [62], the success of the 5 cm rule in treating depression might be explained by engagement of transitional DLPFC regions leading to a different response. The 5 cm targets in our rTMS patients with TRMD were functionally connected with the DMN and showed little anticorrelation with the subgenual cingulate. We observed anticorrelations between 5 cm targets and motor cortex, consistent with reports of inhibitory interactions with paired pulse TMS paradigms [68] and the presence of motor cortex-defined paired-pulse abnormalities in psychiatric illnesses [69]. These anticorrelations may also partially explain how pain responds to rTMS stimulation of both motor cortex targets and 5 cm-defined frontal targets [70].

The seed-based connectivity cluster analyses revealed that posterior cingulate, lateral temporal, and inferior parietal regions belonged to our frontal target networks, hence modulation of these regions by rTMS may have behavioral effects in addition to depression response. Multiple brain regions connect to the metabolically active posterior cingulate which is a central node in the DMN [71] and is involved in attention, Alzheimer's disease,

depression, and other disorders [72]. The lateral temporal regions were part of DMN while the inferior parietal peaks were in either DMN or the ventral attention network.

Our TRMD cohort, a subset of those studied in CSP556, was largely comprised of white men, affecting the generalizability of our results to other ethnicities, women, and the remaining CSP556 participants. However, the homogeneity of our sample likely leads to an underestimation of the effects of head morphometry on fixed rule targeting, and based on the literature comparing 10–20 EEG targets to neuronavigation [8,73–77], there will likely be some residual contribution of head size unaccounted for by registration to an MNI-atlas. Moreover, while we assumed that seed based functional connectivity maps represented networks modulated by TMS stimulation, the variability of frontal cortex networks between individuals limits the value of maps derived from a group average dataset. In addition, our resting-state scans were shorter than current recommendations for stable estimates of resting-state networks [78]. Our work neglected coil orientation, pulse shape, and did not incorporate electric field modeling. Although an exploratory look at the variability of the TMS-induced electric fields revealed no systematic differences in field magnitude or shape due to stimulation location (Fig. S6) that might alter our main conclusion that some rules target different anatomy and networks, we acknowledge that the use of electric field modeling would refine our estimates of subgenual cingulate and seed-based connectivity. Also, our virtually traced rules are idealized targets, and may not correspond to the same rules if traced by a technician in person, as demonstrated by the applied 6 cm rule. Despite these limitations, in the absence of trials comparing targeting methods and depression outcomes, our results support TMS targeting based on EEG electrode locations [35] (see http://clinicalresearcher.org/eeg/) when MR image guidance is unavailable, as these rules consistently targeted DLPFC brain regions with resting-state fMRI features known to be associated with depression response. There have, however, been differences across studies in the MNI coordinates derived from the F3 scalp target [79], and the precise anatomy and networks targeted would differ for other MNI-coordinate definitions of EEG F3. Lastly, we identified other brain systems likely to be modulated by DLPFC targets, potentially enabling clinicians to choose a patient-specific targeting strategy, such as choosing to stimulate a DLPFC subregion that simultaneously modulates the motor network [70] when treating a depressed patient with comorbid pain or the posterior cingulate when treating a patient comorbid for Alzheimer's disease [80]. In summary, our study demonstrates that precision lab-based tracing to identify brain substrates modulated by proposed targets is an approach for neuroepidemiology.

Supplementary Material

Refer to Web version on PubMed Central for supplementary material.

Acknowledgments

Many thanks to the patients and staff of CSP556.

References

[1]. Perera T, George MS, Grammer G, Janicak PG, Pascual-Leone A, Wirecki TS. The clinical TMS society consensus review and treatment recommendations for TMS therapy for major depressive disorder. Brain stimulation 2016;9(3): 336–46. [PubMed: 27090022]

[2]. George MS, Taylor JJ, Short EB. The expanding evidence base for rTMS treatment of depression. Current Opinion in Psychiatry 2013;26(1).

[3]. Guo Q, Li CB, Wang JJ. Updated review on the clinical use of repetitive transcranial magnetic stimulation in psychiatric disorders. Neuroscience Bulletin 2017;33(6):747–56. [PubMed: 29064064]

[4]. Oathes DJ, Balderston NL, Kording KP, DeLuisi JA, Perez GM, Medaglia JD, et al. Combining transcranial magnetic stimulation with functional magnetic resonance imaging for probing and modulating neural circuits relevant to affective disorders. Wiley Interdiscip Rev Cogn Sci; 2021. p. e1553. [PubMed: 33470055]

[5]. Fitzgerald PB, Hoy KE, Anderson RJ, Daskalakis ZJ. A study of the pattern of response to rTMS treatment in depression. Depression and Anxiety 2016;33(8):746–53. [PubMed: 27059158]

[6]. Berlim MT, van den Eynde F, Tovar-Perdomo S, Daskalakis ZJ. Response, remission and drop-out rates following high-frequency repetitive transcranial magnetic stimulation (rTMS) for treating major depression: a systematic review and meta-analysis of randomized, double-blind and sham-controlled trials. Psychological Medicine 2014;44(2):225–39. [PubMed: 23507264]

[7]. Glasser MF, Coalson TS, Robinson EC, Hacker CD, Harwell J, Yacoub E, et al. A multi-modal parcellation of human cerebral cortex. Nature 2016;536(7615): 171–8. [PubMed: 27437579]

[8]. Cash RFH, Zalesky A, Thomson RH, Tian Y, Cocchi L, Fitzgerald PB. Subgenual functional connectivity predicts antidepressant treatment response to transcranial magnetic stimulation: independent validation and evaluation of personalization. Biological Psychiatry 2019;86(2):e5–7. [PubMed: 30670304]

[9]. Weigand A, Horn A, Caballero R, Cooke D, Stern AP, Taylor SF, et al. Prospective validation that subgenual connectivity predicts antidepressant efficacy of transcranial magnetic stimulation sites. Biological Psychiatry 2018;84(1): 28–37. [PubMed: 29274805]

[10]. Fox MD, Buckner RL, White MP, Greicius MD, Pascual-Leone A. Efficacy of transcranial magnetic stimulation targets for depression is related to intrinsic functional connectivity with the subgenual cingulate. Biol Psychiatry 2012;72(7):595–603. [PubMed: 22658708]

[11]. Herbsman T, Avery D, Ramsey D, Holtzheimer P, Wadjik C, Hardaway F, et al. More lateral and anterior prefrontal coil location is associated with better repetitive transcranial magnetic stimulation antidepressant response. Biological Psychiatry 2009;66(5):509–15. [PubMed: 19545855]

[12]. Cash RFH, Weigand A, Zalesky A, Siddiqi SH, Downar J, Fitzgerald PB, et al. Using brain imaging to improve spatial targeting of transcranial magnetic stimulation for depression. Biol Psychiatry 2020.

[13]. Baxter LR Jr, Schwartz JM, Phelps ME, Mazziotta JC, Guze BH, Selin CE, et al. Reduction of prefrontal cortex glucose metabolism common to three types of depression. Arch Gen Psychiatry 1989;46(3):243–50. [PubMed: 2784046]

[14]. Martinot MLP, Galinowski A, Ringuenet D, Gallarda T, Lefaucheur JP, Bellivier F, et al. Influence of prefrontal target region on the efficacy of repetitive transcranial magnetic stimulation in patients with medication-resistant depression: a [(18)F]-fluorodeoxyglucose PET and MRI study. International Journal of Neuropsychopharmacology 2010;13(1):45–59.

[15]. Fitzgerald PB, Oxley TJ, Laird AR, Kulkarni J, Egan GF, Daskalakis ZJ. An analysis of functional neuroimaging studies of dorsolateral prefrontal cortical activity in depression. Psychiatry Res 2006;148(1):33–45. [PubMed: 17029760]

[16]. Brody AL, Saxena S, Mandelkern MA, Fairbanks LA, Ho ML, Baxter LR. Brain metabolic changes associated with symptom factor improvement in major depressive disorder. Biol Psychiatry 2001;50(3):171–8. [PubMed: 11513815]

[17]. George MS, Wassermann EM, Williams WA, Callahan A, Ketter TA, Basser P, et al. Daily repetitive transcranial magnetic stimulation (rTMS) improves mood in depression. Neuroreport 1995;6(14):1853–6. [PubMed: 8547583]

[18]. Pascual-Leone A, Rubio B, Pallardo F, Catala MD. Rapid-rate transcranial magnetic stimulation of left dorsolateral prefrontal cortex in drug-resistant depression. Lancet 1996;348(9022):233–7. [PubMed: 8684201]

[19]. Cieslik EC, Zilles K, Caspers S, Roski C, Kellermann TS, Jakobs O, et al. Is there "one" DLPFC in cognitive action control? Evidence for heterogeneity from co-activation-based parcellation. Cereb Cortex 2013;23(11):2677–89. [PubMed: 22918987]

[20]. George MS, Lisanby SH, Avery D, McDonald WM, Durkalski V, Pavlicova M, et al. Daily left prefrontal transcranial magnetic stimulation therapy for major depressive disorder: a sham-controlled randomized trial. Arch Gen Psychiatry 2010;67(5):507–16. [PubMed: 20439832]

[21]. Avery DH, Holtzheimer PE, Fawaz W, Russo J, Neumaier J, Dunner DL, et al. A controlled study of repetitive transcranial magnetic stimulation in medication-resistant major depression. Biological Psychiatry 2006;59(2): 187–94. [PubMed: 16139808]

[22]. Herwig U, Padberg F, Unger J, Spitzer M, Schonfeldt-Lecuona C. Transcranial magnetic stimulation in therapy studies: examination of the reliability of "standard" coil positioning by neuronavigation. Biol Psychiatry 2001;50(1): 58–61. [PubMed: 11457424]

[23]. Mi Z, Biswas K, Fairchild JK, Davis-Karim A, Phibbs CS, Forman SD, et al. Repetitive transcranial magnetic stimulation (rTMS) for treatment-resistant major depression (TRMD) Veteran patients: study protocol for a randomized controlled trial. Trials 2017;18(1):409. [PubMed: 28865495]

[24]. Fitzgerald PB, Maller J, Hoy KE, Thomson R, Daskalakis ZJ. Exploring the optimal site for the localization of dorsolateral prefrontal cortex in brain stimulation experiments. Brain stimulation 2009;2:234–7. [PubMed: 20633422]

[25]. Ahdab R, Ayache SS, Brugieres P, Goujon C, Lefaucheur JP. Comparison of "standard" and "navigated" procedures of TMS coil positioning over motor, premotor and prefrontal targets in patients with chronic pain and depression. Neurophysiologie Clinique-Clinical Neurophysiology 2010;40(1):27–36. [PubMed: 20230933]

[26]. Trapp NT, Bruss J, King Johnson M, Uitermarkt BD, Garrett L, Heinzerling A, et al. Reliability of targeting methods in TMS for depression: Beam F3 vs. 5.5 cm. Brain stimulation 2020;13(3):578–81. [PubMed: 32289680]

[27]. Evans AC, Collins DL, Mills SR, Brown ED, Kelly RL, Peters TM. 3D statistical neuroanatomical models from 305 MRI volumes. 1993.

[28]. Grabner G, Janke AL, Budge MM, Smith D, Pruessner J, Collins DL. Symmetric atlasing and model based segmentation: an application to the hippocampus in older adults. Lect Notes Comput Sc 2006;4191:58–66.

[29]. Fitzgerald PB, Hoy K, McQueen S, Maller JJ, Herring S, Segrave R, et al. A randomized trial of rTMS targeted with MRI based neuro-navigation in treatment-resistant depression. Neuropsychopharmacology 2009;34(5): 1255–62. [PubMed: 19145228]

[30]. Cash RFH, Cocchi L, Lv J, Wu Y, Fitzgerald PB, Zalesky A. Personalized connectivity-guided DLPFC-TMS for depression: advancing computational feasibility, precision and reproducibility. Hum Brain Mapp 2021;42(13): 4155–72. [PubMed: 33544411]

[31]. Williams NR, Sudheimer KD, Bentzley BS, Pannu J, Stimpson KH, Duvio D, et al. High-dose spaced theta-burst TMS as a rapid-acting antidepressant in highly refractory depression. Brain 2018;141(3):e18–. [PubMed: 29415152]

[32]. Siddiqi SH, Weigand A, Pascual-Leone A, Fox MD. Identification of personalized transcranial magnetic stimulation targets based on subgenual cingulate connectivity: an independent replication. Biological Psychiatry 2021;90(10): e55–6. [PubMed: 33820629]

[33]. Li CT, Cheng CM, Chen MH, Juan CH, Tu PC, Bai YM, et al. Antidepressant efficacy of prolonged intermittent theta burst stimulation monotherapy for recurrent depression and comparison of methods for coil positioning: a randomized, double-blind, sham-controlled study. Biol Psychiatry 2020;87(5): 443–50. [PubMed: 31563272]

[34]. Herwig U, Satrapi P, Schönfeldt-Lecuona C. Using the international 10–20 EEG system for positioning of transcranial magnetic stimulation. Brain Topography 2003;16(2):95–9. [PubMed: 14977202]

[35]. Beam W, Borckardt JJ, Reeves ST, George MS. An efficient and accurate new method for locating the F3 position for prefrontal TMS applications. Brain stimulation 2009;2(1):50–4. [PubMed: 20539835]

[36]. McClintock SM, Reti IM, Carpenter LL, McDonald WM, Dubin M, Taylor SF, et al. Consensus recommendations for the clinical application of repetitive transcranial magnetic stimulation (rTMS) in the treatment of depression. J Clin Psychiatry 2018;79(1).

[37]. Mir-Moghtadaei A, Caballero R, Fried P, Fox MD, Lee K, Giacobbe P, et al. Concordance between BeamF3 and MRI-neuronavigated target sites for repetitive transcranial magnetic stimulation of the left dorsolateral prefrontal cortex. Brain stimulation 2015;8(5):965–73. [PubMed: 26115776]

[38]. Bestmann S, Baudewig J, Siebner HR, Rothwell JC, Frahm J. Functional MRI of the immediate impact of transcranial magnetic stimulation on cortical and subcortical motor circuits. Eur J Neurosci 2004;19(7):1950–62. [PubMed: 15078569]

[39]. Beynel L, Powers JP, Appelbaum LG. Effects of repetitive transcranial magnetic stimulation on resting-state connectivity: a systematic review. Neuroimage 2020:211.

[40]. Siddiqi SH, Trapp NT, Hacker CD, Laumann TO, Kandala S, Hong X. Repetitive transcranial magnetic stimulation with resting-state network targeting for treatment-resistant depression in traumatic brain injury: a randomized, controlled, double-blinded pilot study. J Neurotrauma 2019;36.

[41]. Cole EJ, Stimpson KH, Bentzley BS, Gulser M, Cherian K, Tischler C, et al. Stanford accelerated intelligent neuromodulation therapy for treatment-resistant depression. Am J Psychiatry 2020;177(8):716–26. [PubMed: 32252538]

[42]. Hawco C, Voineskos AN, Steeves JKE, Dickie EW, Viviano JD, Downar J, et al. Spread of activity following TMS is related to intrinsic resting connectivity to the salience network: a concurrent TMS-fMRI study. Cortex 2018;108: 160–72. [PubMed: 30195825]

[43]. Philip NS, Barredo J, van 't Wout-Frank M, Tyrka AR, Price LH, Carpenter LL. Network mechanisms of clinical response to transcranial magnetic stimulation in posttraumatic stress disorder and major depressive disorder. Biological Psychiatry 2018;83(3):263–72. [PubMed: 28886760]

[44]. Yeo BTT, Krienen FM, Sepulcre J, Sabuncu MR, Lashkari D, Hollinshead M, et al. The organization of the human cerebral cortex estimated by intrinsic functional connectivity. Journal of Neurophysiology 2011;106(3):1125–65. [PubMed: 21653723]

[45]. Yesavage JA, Fairchild JK, Mi Z, Biswas K, Davis-Karim A, Phibbs CS, et al. Effect of repetitive transcranial magnetic stimulation on treatment-resistant major depression in US Veterans: a randomized clinical trial. JAMA Psychiatry 2018;75(9):884–93. [PubMed: 29955803]

[46]. Yousry TA, Schmid UD, Alkadhi H, Schmidt D, Peraud A, Buettner A, et al. Localization of the motor hand area to a knob on the precentral gyrus. A new landmark. Brain 1997;120(Pt 1):141–57. [PubMed: 9055804]

[47]. Bungert A, Antunes A, Espenhahn S, Thielscher A. Where does TMS stimulate the motor cortex? Combining electrophysiological measurements and realistic field estimates to reveal the affected cortex position. Cerebral Cortex 2017;27(11):5083–94. [PubMed: 27664963]

[48]. Rorden C, Karnath HO, Bonilha L. Improving lesion–symptom mapping. Journal of Cognitive Neuroscience 2007;19(7):1081–8. [PubMed: 17583985]

[49]. Johnson RA, Wichern DW. Applied multivariate statistical analysis. sixth ed. Upper Saddle River, N.J.: Pearson Prentice Hall; 2007.

[50]. Behzadi Y, Restom K, Liau J, Liu TT. A component based noise correction method (CompCor) for BOLD and perfusion based fMRI. NeuroImage 2007;37(1):90–101. [PubMed: 17560126]

[51]. Murphy K, Birn RM, Handwerker DA, Jones TB, Bandettini PA. The impact of global signal regression on resting state correlations: are anti-correlated networks introduced? NeuroImage 2009;44(3):893–905. [PubMed: 18976716]

[52]. Saad ZS, Gotts SJ, Murphy K, Chen G, Jo HJ, Martin A, et al. Trouble at rest: how correlation patterns and group differences become distorted after global signal regression. Brain Connect 2012;2(1):25–32. [PubMed: 22432927]

[53]. Chai XJ, Castanon AN, Ongur D, Whitfield-Gabrieli S. Anticorrelations in resting state networks without global signal regression. Neuroimage 2012;59(2):1420–8. [PubMed: 21889994]

[54]. Cao J, Worsley K. The geometry of correlation fields with an application to functional connectivity of the brain. The annals of applied probability 1999;9(4):1021–57.

[55]. Worsley KJ, Chen JI, Lerch J, Evans AC. Comparing functional connectivity via thresholding correlations and singular value decomposition. Philos Trans R Soc Lond B Biol Sci 2005;360(1457):913–20. [PubMed: 16087436]

[56]. Nichols TE, Holmes AP. Nonparametric permutation tests for functional neuroimaging: a primer with examples. Hum Brain Mapp 2002;15(1):1–25. [PubMed: 11747097]

[57]. Cox RW. AFNI: software for analysis and visualization of functional magnetic resonance neuroimages. Comput Biomed Res 1996;29(3):162–73. [PubMed: 8812068]

[58]. Forman SD, Cohen JD, Fitzgerald M, Eddy WF, Mintun MA, Noll DC. Improved assessment of significant activation in functional magnetic resonance imaging (fMRI): use of a cluster-size threshold. Magn Reson Med 1995;33(5):636–47. [PubMed: 7596267]

[59]. Cox RW, Chen G, Glen DR, Reynolds RC, Taylor PA. FMRI clustering in AFNI: false-positive rates redux. Brain Connectivity 2017;7(3):152–71. [PubMed: 28398812]

[60]. Zou KH, Warfield SK, Bharatha A, Tempany CM, Kaus MR, Haker SJ, et al. Statistical validation of image segmentation quality based on a spatial overlap index. Acad Radiol 2004;11(2):178–89. [PubMed: 14974593]

[61]. Ahdab R, Ayache SS, Brugières P, Farhat WH, Lefaucheur J-P. The hand motor hotspot is not always located in the hand knob: a neuronavigated transcranial magnetic stimulation study. Brain Topography 2016;29(4):590–7. [PubMed: 26980192]

[62]. Johnson KA, Baig M, Ramsey D, Lisanby SH, Avery D, McDonald WM, et al. Prefrontal rTMS for treating depression: location and intensity results from the OPT-TMS multi-site clinical trial. Brain stimulation 2012;6(2):108–17. [PubMed: 22465743]

[63]. Seeley WW, Menon V, Schatzberg AF, Keller J, Glover GH, Kenna H, et al. Dissociable intrinsic connectivity networks for salience processing and executive control. Journal of Neuroscience 2007;27(9):2349–56. [PubMed: 17329432]

[64]. Dosenbach NU, Fair DA, Cohen AL, Schlaggar BL, Petersen SE. A dual-networks architecture of top-down control. Trends Cogn Sci 2008;12(3):99–105. [PubMed: 18262825]

[65]. Mylius V, Ayache SS, Ahdab R, Farhat WH, Zouari HG, Belke M, et al. Definition of DLPFC and M-1 according to anatomical landmarks for navigated brain stimulation: inter-rater reliability, accuracy, and influence of gender and age. Neuroimage 2013;78:224–32. [PubMed: 23567888]

[66]. Gugino LD, Romero JR, Aglio L, Titone D, Ramirez M, Pascual-Leone A, et al. Transcranial magnetic stimulation coregistered with MRI: a comparison of a guided versus blind stimulation

technique and its effect on evoked compound muscle action potentials. Clin Neurophysiol 2001;112(10):1781–92. [PubMed: 11595135]

[67]. Siddiqi SH, Taylor SF, Cooke D, Pascual-Leone A, George MS, Fox MD. Distinct symptom-specific treatment targets for circuit-based neuromodulation. Am J Psychiatry 2020;177(5):435–46. [PubMed: 32160765]

[68]. Ni Z, Gunraj C, Nelson AJ, Yeh IJ, Castillo G, Hoque T, et al. Two phases of interhemispheric inhibition between motor related cortical areas and the primary motor cortex in human. Cereb Cortex 2009;19(7):1654–65. [PubMed: 19015374]

[69]. Radhu N, de Jesus DR, Ravindran LN, Zanjani A, Fitzgerald PB, Daskalakis ZJ. A meta-analysis of cortical inhibition and excitability using transcranial magnetic stimulation in psychiatric disorders. Clinical Neurophysiology 2013;124(7):1309–20. [PubMed: 23485366]

[70]. de Andrade DC, Mhalla A, Adam F, Texeira MJ, Bouhassira D. Neuropharmacological basis of rTMS-induced analgesia: the role of endogenous opioids. Pain 2011;152(2):320–6. [PubMed: 21146300]

[71]. Buckner RL, Andrews-Hanna JR, Schacter DL. The brain's default network -anatomy, function, and relevance to disease. Year in Cognitive Neuroscience 2008 2008;1124:1–38.

[72]. Leech R, Sharp DJ. The role of the posterior cingulate cortex in cognition and disease. Brain 2014;137(Pt 1):12–32. [PubMed: 23869106]

[73]. De Witte S, Klooster D, Dedoncker J, Duprat R, Remue J, Baeken C. Left prefrontal neuronavigated electrode localization in tDCS: 10e20 EEG system versus MRI-guided neuronavigation. Psychiatry Research: Neuroimaging 2018;274:1–6. [PubMed: 29429773]

[74]. Okamoto M, Dan H, Sakamoto K, Takeo K, Shimizu K, Kohno S, et al. Three-dimensional probabilistic anatomical cranio-cerebral correlation via the international 10e20 system oriented for transcranial functional brain mapping. Neuroimage 2004;21(1):99–111. [PubMed: 14741647]

[75]. Seibt O, Brunoni AR, Huang Y, Bikson M. The pursuit of DLPFC: non-neuronavigated methods to target the left dorsolateral pre-frontal cortex with symmetric bicephalic transcranial direct current stimulation (tDCS). Brain stimulation 2015;8(3):590–602. [PubMed: 25862601]

[76]. Herwig U, Satrapi P, Schoenfeldt-Lecuona C. Using the international 10–20 EEG system for positioning of transcranial magnetic stimulation. Brain Topography 2003;16(2):95–9. [PubMed: 14977202]

[77]. Koessler L, Maillard L, Benhadid A, Vignal JP, Felblinger J, Vespignani H, et al. Automated cortical projection of EEG sensors: anatomical correlation via the international 10e10 system. NeuroImage 2009;46(1):64–72. [PubMed: 19233295]

[78]. Laumann Timothy O, Gordon Evan M, Adeyemo B, Snyder Abraham Z, Joo Sung J, Chen M-Y, et al. Functional system and areal organization of a highly sampled individual human brain. Neuron 2015;87(3):657–70. [PubMed: 26212711]

[79]. Fitzgerald PB. Targeting repetitive transcranial magnetic stimulation in depression: do we really know what we are stimulating and how best to do it? Brain Stimul. 2021;14(3):P730–6.

[80]. Minoshima S, Giordani B, Berent S, Frey KA, Foster NL, Kuhl DE. Metabolic reduction in the posterior cingulate cortex in very early Alzheimer's disease. Annals of Neurology: Official Journal of the American Neurological Association and the Child Neurology Society 1997;42(1):85–94.
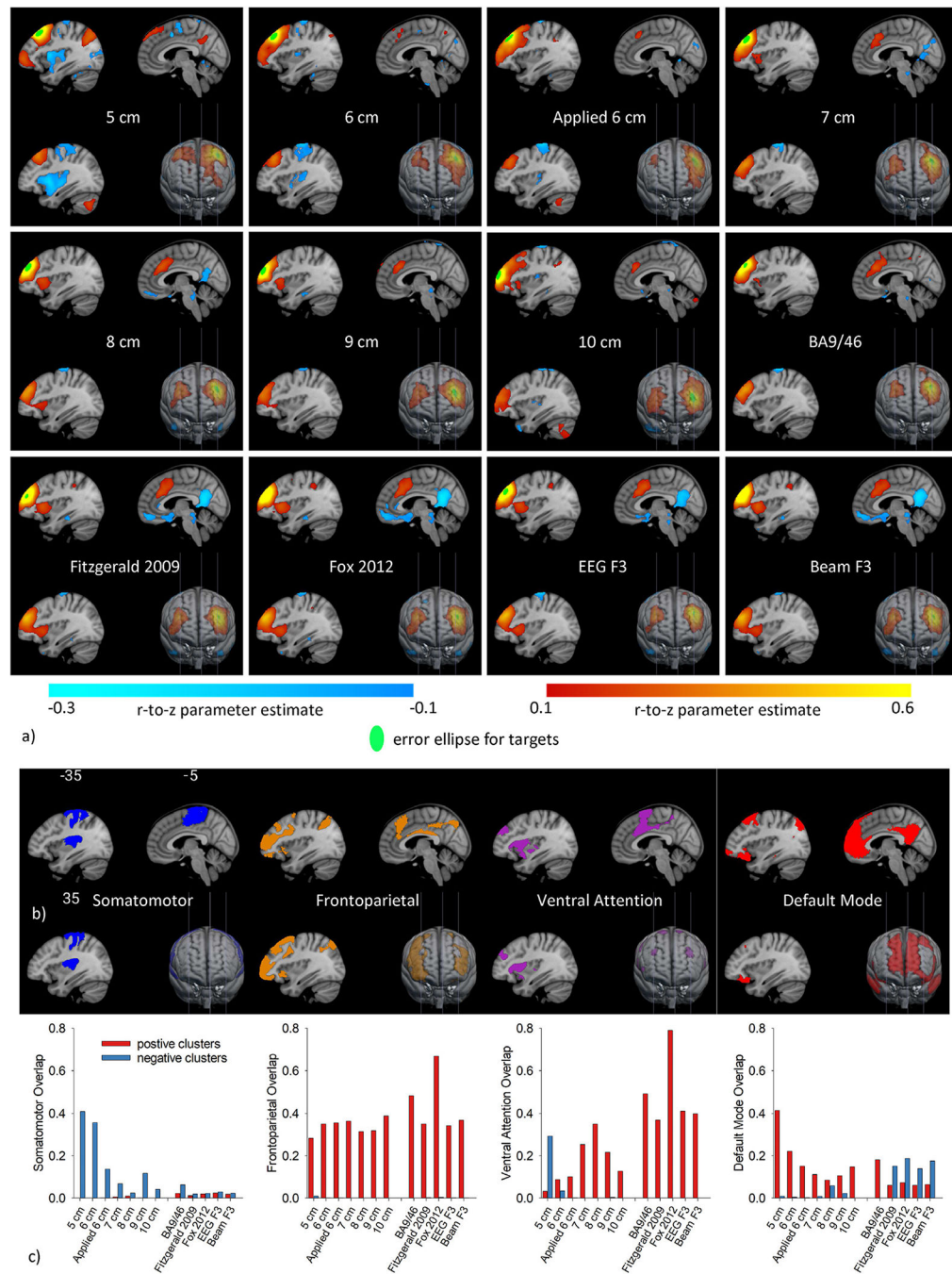
Fig. 1.
a) Resting-state networks (average r-to-z across maps generated from 10 mm spherical seeds placed at each individual's virtual target correlated with all other voxels) for each rule at 3 sagittal slices (MNI x = −35, −5, and 5 mm) and a 3D view from the front. Only significant (corrected on cluster size, $p < 0.05$) connections with magnitude greater than 0.1 are displayed. Overlaid on the maps is the green error ellipse showing the average location and dispersion of target centers across patients for each rule. b) The spatial distribution of the somatomotor, frontoparietal, ventral attention, and default mode networks as defined by

Yeo. c) Bar graphs of the dice overlap between resting-state networks connected to each rule's virtually traced targets and the Yeo networks.
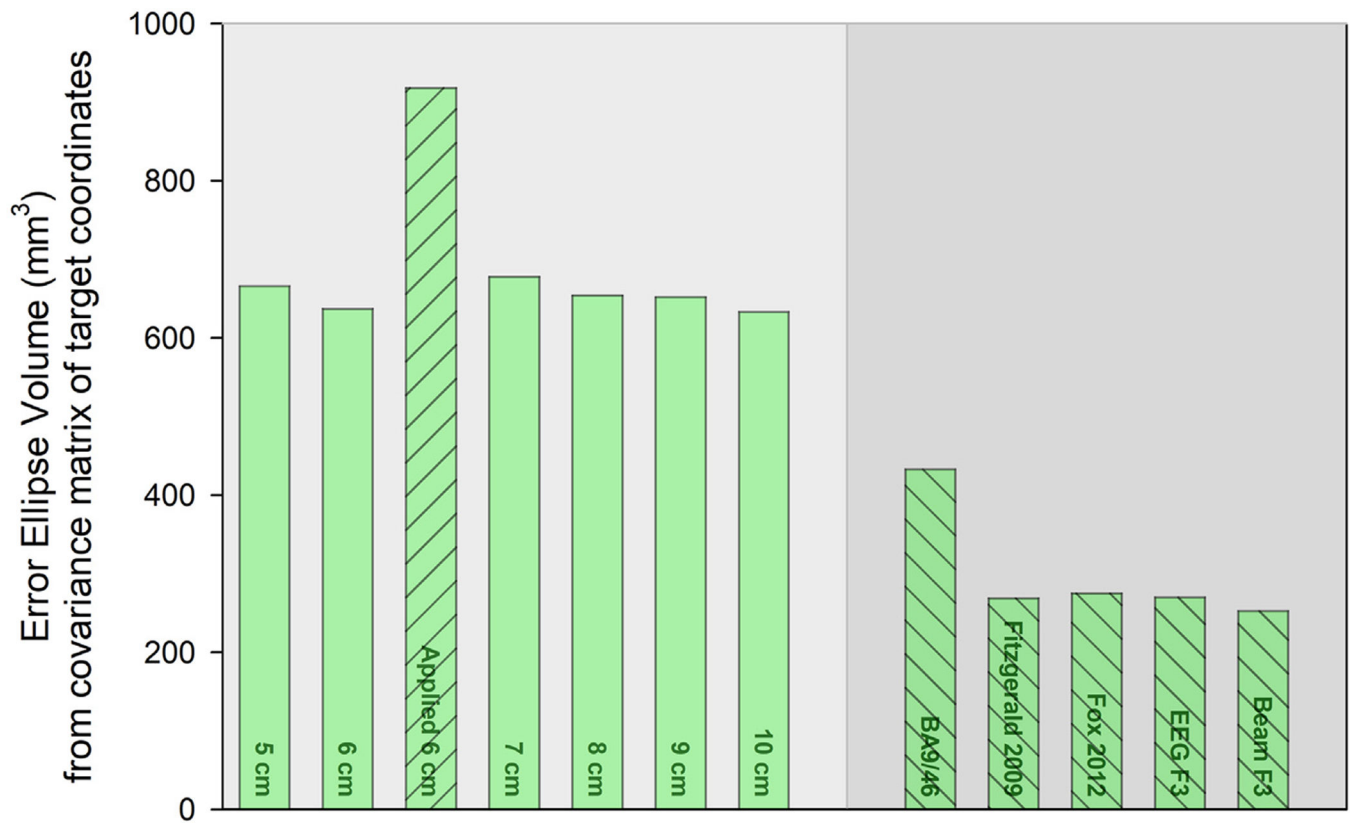
Fig. 2.
Bar height denotes the error ellipse volume for each rule. Rules with equivalent covariance matrices have the same bar pattern. For example, the Applied 6 cm rule bar has upward sloping lines, and is different from the equivalent other fixed distance rules (no pattern) and the equivalent adjusted rules (downward sloping lines).
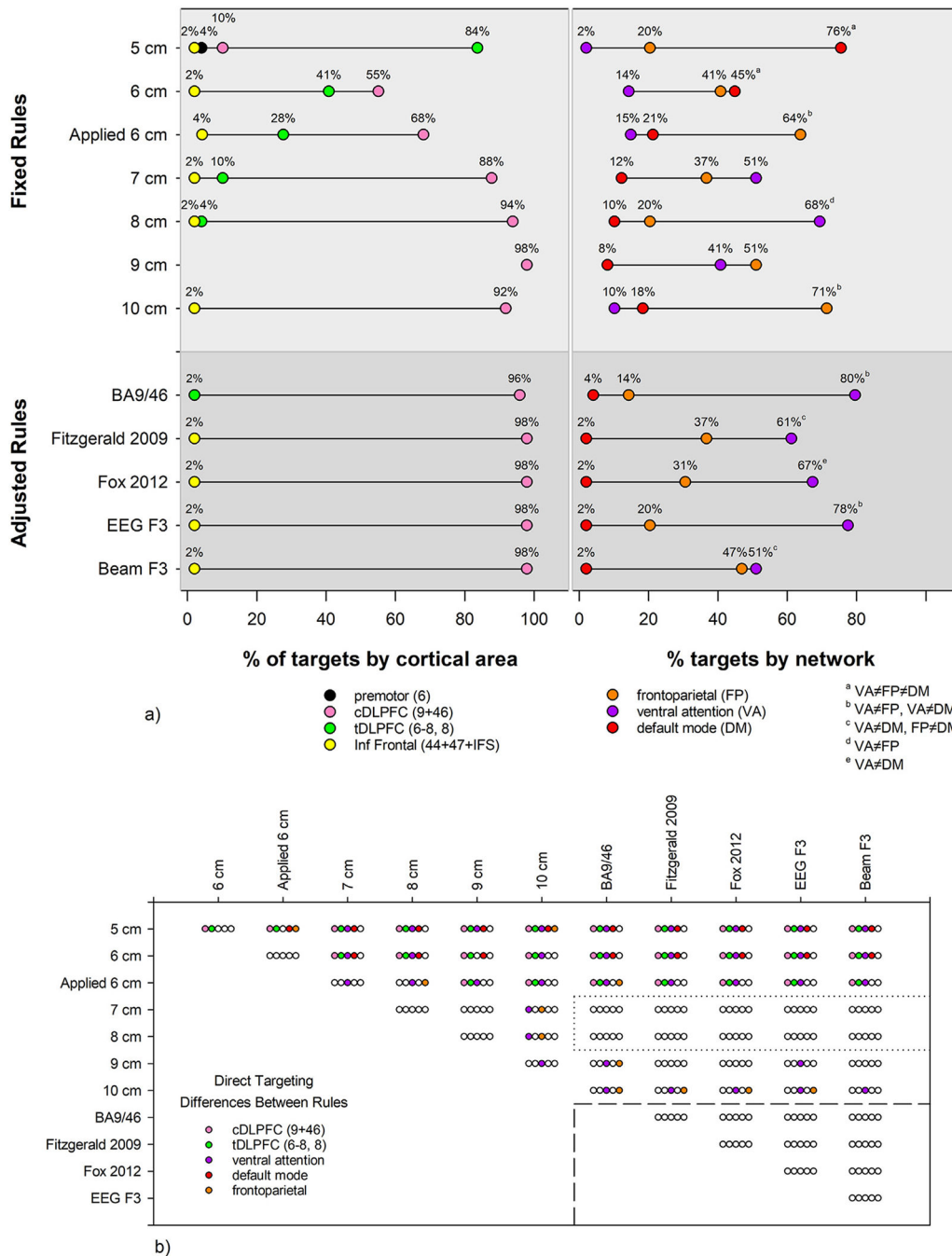
Fig. 3.
a) For each rule, the percentage of locations within HCP anatomical structure (left) and Yeo-7 network (right) is displayed. tDLPFC: transitional dorsolateral prefrontal cortex, Areas 8, 6–8; cDLPFC: classical dorsolateral prefrontal cortex, Areas 9 and 46; Inf Frontal: inferior frontal. The percentage of targets in tDLPFC and cDLPFC were different for all rules. For the % targets by network, superscript letters denote which networks were differently targeted for each rule, i.e. the 5 cm preferentially targets the default mode network, because the % of targets in the ventral attention, frontoparietal, and default mode

networks are all significantly different. b) The results of χ^2 tests, corrected for multiple comparisons, are shown. Each set of 5 bubbles shows whether the percentage of targets are different between the row and column rules labels, where an empty bubble means no difference. For example, the top left set of bubbles compares the 5 and 6 cm rules, with a difference in the percentage of targets in cDLPFC and tDLPFC, and no difference in networks targeted. Note that the 7, 8, and adjusted rules show no differences with each other in direct targeting of anatomy or networks.
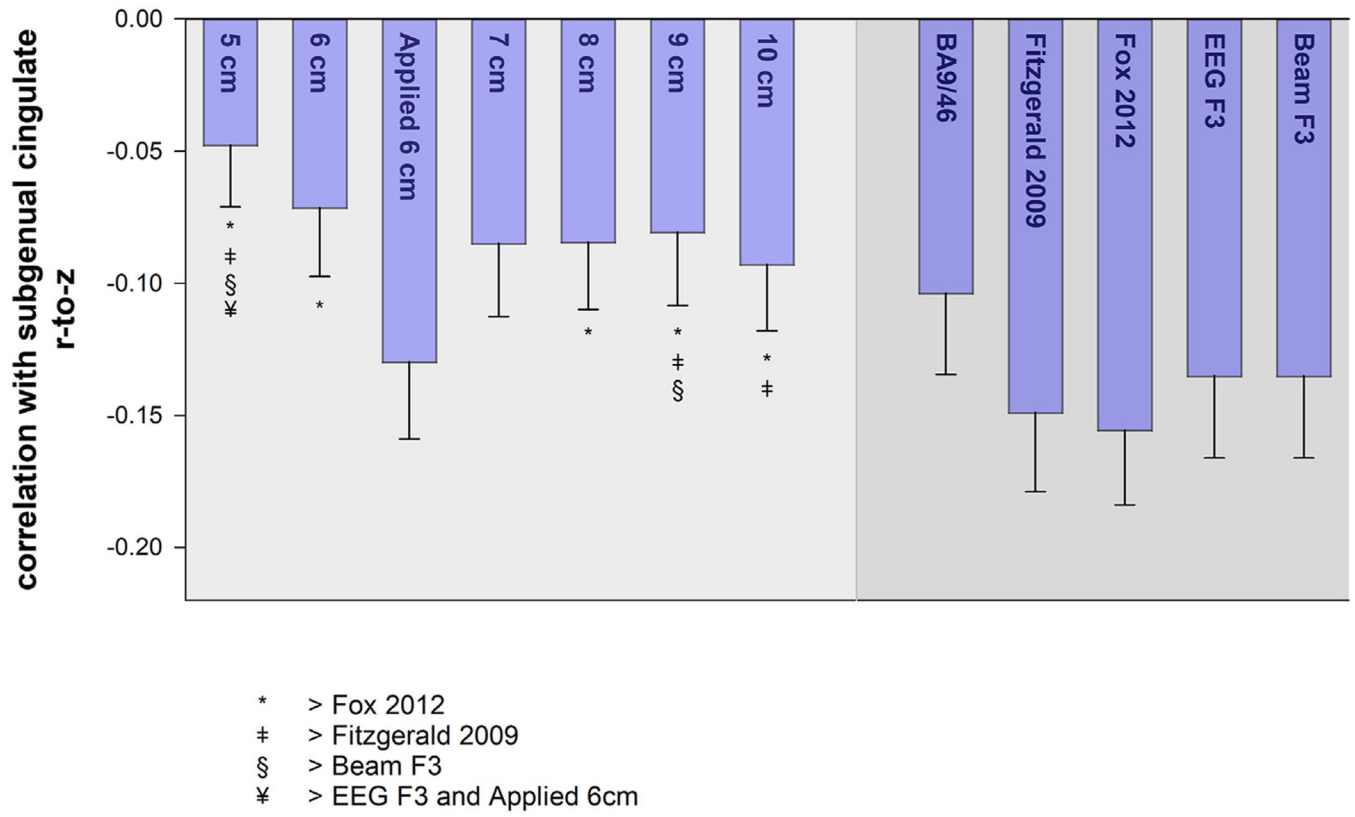
*   > Fox 2012
‡   > Fitzgerald 2009
§   > Beam F3
¥   > EEG F3 and Applied 6cm

Fig. 4.
Bars show the average correlation ± standard error between the subgenual cingulate and targets for each rule. Symbols denote rules with larger correlations (i.e., smaller anticorrelations).

Table 1

Patient demographics.

	Mean (SD) or n (%) N = 49
Age	55.96 (11.93)
Sex, Male	39 (79.59)
Education (N = 42)	13.9 (1.96)
Race, Caucasian	40 (81.63)
BDI-II Score (N = 43)	23.3 (10.26)
PTSD (PCL-M) (N = 43)	42.67 (17.3)

Note: BDI-II= Beck Depression Inventory - II, PCL-M = PTSD Checklist-Military Version.